

L183 (L134N) Revisited

I. The very cold core and the ridge[★]

L. Pagani¹, G. Lagache², A. Bacmann³, F. Motte⁴, L. Cambrézy⁵, M. Fich⁶, D. Teyssier⁷,
M.-A. Miville-Deschênes^{2,8}, J.-R. Pardo⁹, A. J. Apponi¹⁰, and B. Stepnik²

¹ LERMA, UMR 8112 du CNRS, Observatoire de Paris, 61 Av. de l'Observatoire, 75014 Paris, France

² IAS, Bât. 121, Université Paris-Sud, 91435 Orsay, France

³ ESO, Karl-Schwarzschild-Str. 2, 85748 Garching bei München, Germany

⁴ CEA, DSM, DAPNIA, Service d'Astrophysique, CE Saclay, 91191 Gif-sur-Yvette Cedex, France

⁵ Observatoire Astronomique de Strasbourg, UMR 7550, Université Louis Pasteur, 67000 Strasbourg, France

⁶ Physics Department, University of Waterloo, Waterloo, Ontario, N2L 3G1, Canada

⁷ SRON, PO Box 800, 9700 AV Groningen, The Netherlands

⁸ CITA, University of Toronto, 60 St. George Street, Toronto, Ontario, M5S 3H8, Canada

⁹ Instituto de Estructura de la Materia, Dpto de Física Molecular CSIC, Madrid, Spain

¹⁰ University of Arizona, Steward Observatory, 933 N. Cherry Ave., Tucson, AZ 85721, USA

Received 24 March 2003 / Accepted 14 June 2003

Abstract. We report new 1.2 mm continuum observations of the L183 (=L134N) dark cloud with the MAMBO bolometer array at IRAM. Combined with ISOCAM and ISOPHOT data at 7 and 200 μm , this new observation is not compatible with the results found by Ward-Thompson et al. (1994) with SCUBA and further analysed by Lehtinen et al. (2003) using ISOPHOT data. Only one bright core, with a northern elongation (the ridge) is detected. We show that this core has an average temperature $T \approx 7.6 \text{ K} \pm 0.5 \text{ K}$ which is one of the coldest temperatures reported so far.

Key words. ISM: dust, extinction – ISM: structure – ISM: individual: L134N – ISM: individual: L183

1. Introduction

L183 is a cold, dark, starless cloud, ideally situated for detailed studies. Due to its high galactic latitude ($b = +37^\circ$), it is not polluted by other cloud emission (especially in continuum) and its proximity ($110 \pm 10 \text{ pc}$, Franco 1989) provides a high linear resolution ($1'' = 110 \text{ AU}$). In previous studies, a 15 K dust region has been detected based on IRAS FIR observations (Laureijs et al. 1991, 1995), and colder dust peaks were identified at $\lambda = 0.85 \text{ mm}$ with JCMT bolometers (Ward-Thompson et al. 1994, hereafter WT94, 2000). Based on these data and ISOPHOT maps, Lehtinen et al. (2003, hereafter LML03) present four cold condensations. However we cannot confirm the existence of all of their sources.

This Letter, the first of a series on this source (see also Pagani et al. 2002, 2003a), reports the results of a combined mid-, far-infrared and millimeter continuum study of

the pre-stellar core of L183 as detected for the first time by Ward-Thompson et al. (2000) and on the extended ridge north of it. Section 2 presents the observations and briefly describes the data reduction while Sect. 3 discusses the critical ISOPHOT data reduction in detail and the general results.

2. Observations

The ISOCAM LW2 (5.0–8.5 μm filter) data and all the ISOPHOT data have been imported from the ISO Data Archive¹. The ISOCAM LW2 map covers $5' \times 5'$ with $6'' \times 6''$ pixels. The data have been reduced following the method described in Miville-Deschênes et al. (2000). Thanks to the data redundancy and oversampling, the final map can be presented with pixels of $3'' \times 3''$. The rms noise in the central part of the map is 0.005 MJy/sr. A 2MASS bright star detected in the upper right corner of the map has allowed us to correct the pointing to better than $1''$. These ISOCAM data are presented here for the first time.

The ISOPHOT data represent two $30' \times 30'$ maps at 100 and 200 μm (see LML03) and a series of declination strips from 100

Send offprint requests to: L. Pagani,
e-mail: laurent.pagani@obspm.fr

[★] Based on observations made with the IRAM-30m and ISO, an ESA project with instruments funded by ESA Member States (especially the PI countries: France, Germany, The Netherlands and the United Kingdom) with the participation of ISAS and NASA.

¹ <http://www.iso.vilspa.esa.es/ida/index.html>

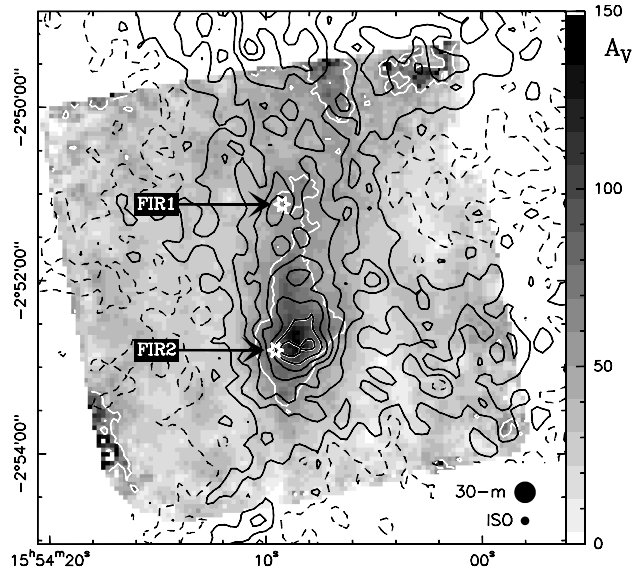


Fig. 1. Image of the core and the ridge in L183. Dust visible extinction (from the ISOCAM $7\ \mu\text{m}$ map, grey plot) and emission at $1.2\ \text{mm}$ (black contours). The image is labelled in absolute (J2000) coordinates. The white contour marks $A_V = 60$ mag. The $1.2\ \text{mm}$ flux levels are: 4.5 (dashed, 5σ), 7 to 22 by steps of 2.5 (3σ) MJy/sr. Beam sizes are indicated in the lower right corner. FIR1 and FIR2 indicate the LML03 source positions.

to $200\ \mu\text{m}$ (see Ward-Thompson et al. 2002, LML03). We have used the latest PIA V10.0 reduction package to analyze them (see Sect. 3.2).

The MAMBO (MPIfR bolometer array on the IRAM 30-m, observing at $1.2\ \text{mm}$ with $11''$ resolution) data were taken in December 2001 (117 channel camera) and February 2002 (37 channel camera). We used the fast-mapping approach described by Teyssier & Sievers (1999), consisting of multiple fast scans of a large area ($15' \times 15'$), each scan lasting approximately 75 min. The fast raster maps consisted of azimuthal scans at a velocity of $8''\ \text{s}^{-1}$ with elevation steps of $24''$ between each scan. For each map, we used different wobbler throws (between $40''$ and $80''$), and various scanning direction to minimize the striping effects. Pointing and sky opacity were checked before and after each map. The typical pointing errors were $3''$ and the zenith atmospheric opacity was in the range 0.1–0.3. The data have been reduced with NIC, the IRAM bolometer package (Broguière et al. 1995) and a skynoise reduction technique described in Motte et al. (2003). The final rms is $0.8\ \text{MJy/sr}$ on the map smoothed to $15''$ resolution. Systematic errors in the baseline level might be larger than that because large scale ($>15'$) features of the map are lost due to the dual-beam mapping and reduction techniques. We have however estimated that the peak emission cannot be underestimated by more than $2\ \text{MJy/sr}$. The absolute calibration uncertainty is estimated to be $\sim 20\%$.

CFHT deep images using the CFHT-IR camera in bands H and K' have been obtained in June 2002. These data are presented elsewhere (Pagani et al. 2003a,b) but are used here to calibrate the ISOCAM data in terms of extinction (A_V , see Sect. 3.1).

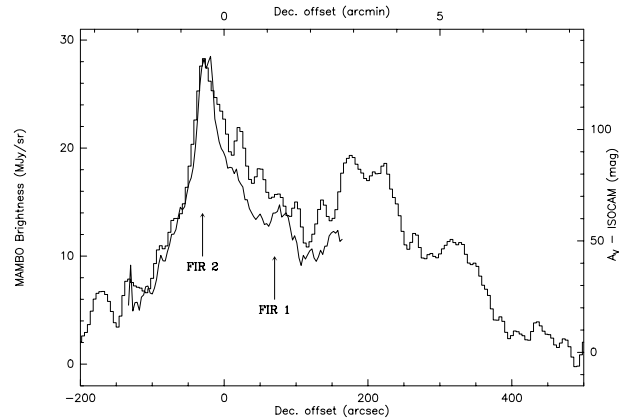


Fig. 2. Vertical cut through the core and the ridge. Dust extinction (from ISOCAM, normal plot) and emission at $1.2\ \text{mm}$ (histogram). Offsets are relative to $\delta_{2000} = -2^\circ 52' 18''$. FIR1 and FIR2 indicate the LML03 source positions.

Finally, we also mapped the source with SCUBA at 850 and $450\ \mu\text{m}$ in Feb. 2001 with a limited success due to medium-quality weather. The $850\ \mu\text{m}$ map, of similar size to the MAMBO map, shows the same emission features but with more noise.

3. Results and discussion

3.1. The core and the ridge

Figure 1 presents the MAMBO $1.2\ \text{mm}$ map (contours) superimposed on an image of A_V derived from the ISOCAM data. The ISOCAM $7\ \mu\text{m}$ absorption map has been converted to a visible extinction map using the method described in detail by Bacmann et al. (2000) except that the conversion has been done using an $H - K'$ infrared excess map (Cambrésy et al. 2002 after Lada et al. 1994) instead of using dust emission and C^{18}O measurements. The result is thus independent of the actual dust temperature and of possible CO depletion. Two regions *outside the main peak* with two different visual extinctions (known from $H - K'$ measurements) are chosen to set the zero and the slope of the conversion. This method implies that the features seen in the image are due to the absorption from the core only, and not to structure in the mid-infrared background or foreground emission. We estimate the random uncertainty on the calibration to be 7% but the global conversion suffers from the critical estimate of the foreground and background infrared emission (see Bacmann et al. 2000) and the total uncertainty on the absolute extinction reaches $+66/-33\%$ at the peak ($A_V \approx 150$ mag). Figures 1 and 2 show very good agreement between MAMBO and ISOCAM data. We clearly see a main peak with an elongated feature north-south which extends in fact beyond the ISOCAM image up to $6'$ north ($\delta_{2000} = -2^\circ 48'$) as revealed by the cut in Fig. 2. This long ridge and the peak have remained completely opaque to K' deep exposures, putting a lower limit of ~ 40 mag to the A_V extinction in that region (see Fig. 2 in Pagani et al. 2003a).

The most striking feature in these ISOCAM and MAMBO maps is the almost total absence of the LML03 source FIR1 while our peak position is nicely correlated with LML03 source

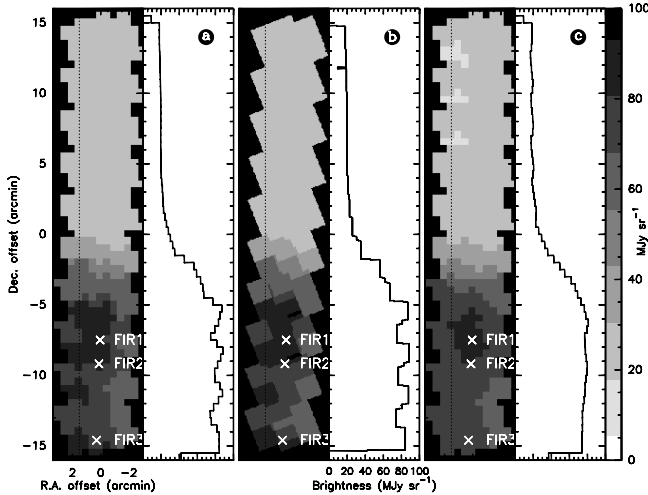


Fig. 3. ISOPHOT strip at $200\ \mu\text{m}$. For each strip a cut at $\Delta\alpha = +1.5'$ is displayed aside. **a)** Timelines flat-fielded in the most diffuse parts of the cloud and projected on a $30''$ grid. **b)** Same as **a)** but projected on a $3''$ grid. **c)** Timelines flat-fielded on the brightest parts of the cloud. Reference position: $\alpha_{2000} = 15\text{h}54\text{m}09.1\text{s}$, $\delta_{2000} = -2^{\circ}43'37.2''$. LML03 sources FIR1–3 are indicated.

FIR2 (despite an apparent $10\text{--}15''$ offset between the two, see Figs. 1 and 2). We estimate, from the Fig. 2b of LML03, a $200\ \mu\text{m}$ peak flux ratio $I_{\text{FIR1}}/I_{\text{FIR2}}$ of about 2.7. As the two sources have almost the same temperature, their submm peak flux ratio is almost the same, i.e. ~ 2.3 (this is confirmed by the FIR1 and FIR2 $L_{\text{sub-mm}}$ values in LML03 Table 4 when the surface ratio $S_{\text{FIR1}}/S_{\text{FIR2}} = 1/3$ is taken into account). In our MAMBO map, source FIR1 is not clearly detected, leading to a ratio $I_{\text{FIR1}}/I_{\text{FIR2}}$ of about 0.55. ISOCAM observations, as well as our large scale SCUBA maps (that are in good agreement with unpublished data from J. Kirk, private communication) confirm this result with a ratio of about 0.45. Though the fluxes measured by WT94 are roughly compatible with ours, we think that they have mistakenly interpreted a piece of the ridge as a point source. We also think that the relative properties of the FIR1 and FIR2 sources described in LML03 are not correct, the FIR1/FIR2 peak flux ratio being weaker than reported by a factor of $2.3/0.5 \approx 5$ (as far as FIR1 can be considered as a point source).

3.2. Are there several point sources in the ISOPHOT strip?

In contrast to the ISOPHOT $200\ \mu\text{m}$ map, the $200\ \mu\text{m}$ strip benefited from a partial oversampling which helped LML03 to cross-identify the FIR1, FIR2 and FIR3 sources. In their work, FIR3 has been detected directly on the ISOPHOT maps. For FIR1 and FIR2, they showed that the 2 sources can be detected as separate sources on the strip and measure their fluxes in the timeline data. We show here that the residual ISOPHOT flat-field pattern prevents the detection of two sources in the core (FIR1 and 2) and could have artificially created FIR3.

ISOPHOT C200 data were carefully reduced using PIA V10.0 (Gabriel et al. 1997) from the Edited

Raw Data (ERD) to the Astrophysical and Application Products (AAP) level. The AAP data were then corrected from the flat-field and projected on the sky using our own procedures. We use two methods to correct for the flat-field: (i) we compute the mean responsivity of the four pixels (by simply averaging the 4 pixel timelines). The flat-field is then given by correlating the AAP brightness timelines of the 4 pixels with the mean responsivity. The correlation can be done on selected parts of the strip i.e. $B_{\text{min}} < B < B_{\text{max}}$ (ii) we project on the sky the raw AAP data, smooth the strip to remove at first order the flat-field pattern, then simulate ISOPHOT observations of the smoothed strip (obtain “smoothed” timelines) and compare the raw AAP and the “smoothed” timelines. Again, the comparison can be done only for selected parts of the strip and this process can then be iterative. The results of the two methods are identical and very close to those obtained with PIA. The flat-field has to be computed in the most diffuse parts of the image (i.e. the low brightness parts), where we assume that the different pixels have observed the same sky (in absence of redundancy, this is the only way to compute the flat-field). For L183 at $200\ \mu\text{m}$, the diffuse parts are chosen as $B < 35\ \text{MJy/sr}$ (results are not sensitive to this value as long as we avoid the bright core).

It appears for L183 that the diffuse part of the strip was efficiently corrected for the flat-field but not the brightest part (the core). This is also true for the larger map. The flat pattern is not easily detectable when the data are projected on a $30''$ grid (as in LML03 and Fig. 3a) but is clearly visible when data are projected on a $3''$ grid without any interpolation (see Fig. 3b)². In this case, four sources are detected in the strip; they are artificially created by a flat-field correction that fails to correct the bright pixels. When we compute the flat-field in the bright part of the cloud ($65 < B < 83\ \text{MJy/sr}$) only one ISOPHOT source (with an extension to the north) is detected in the strip (Fig. 3c), but in this case the diffuse parts of the map clearly exhibit residual flat-field effects. Therefore, it is clear that the flat-field varies in these observations, leading to a systematic error up to 15% of the pixel intensity. This variation prevents the detection of point sources in these ISOPHOT data, as illustrated in Fig. 3.

3.3. Dust temperature of the core and the ridge

Using ISOCAM data as a reference, we are going to evaluate T_{dust} for both the core and the ridge from the ISOPHOT and the MAMBO map data. For the ISOPHOT data, the background has been subtracted by scaling the IRAS $60\ \mu\text{m}$ emission to the cloud-free part of the ISOPHOT maps.

If we smooth and reproject either the MAMBO, SCUBA or ISOCAM data to the ISOPHOT $200\ \mu\text{m}$ resolution ($\approx 90''$) and grid, we still see the core as a prominent peak, stronger than the ridge. This is not the case in the ISOPHOT map at $200\ \mu\text{m}$ (LML03) where the emission obviously reveals the ridge but

² Note that the very thin gridding gives an accurate image of the original pixels projected in the Ra-Dec frame and thus Fig. 3b looks coarser than Fig. 3a. This illustrates how misleading the $30''$ reprojecting is.

slightly drops where the core is expected, south of it. The most probable explanation for this difference between these maps and ISOPHOT maps is that the inner core dust is too cold to bring a measurable contribution to the 200 μm emission and also that the core must be colder than the ridge. The 100 μm emission map does not trace the ridge and the core at all, indicating that all the ridge and the core must be below 10 K. It traces instead a thin warm layer surrounding them. While the 100 μm emission comes solely from this warm layer, it is difficult to assess the percentage of 200 μm emission coming from that layer. This requires to know the temperature profile of the dust. A first, coarse approach can be attempted using Zucconi et al. (2001) Eqs. (21)–(26) to compute the temperature profile and the 100 and 200 μm emissions. Using these equations, we have considered the ISOPHOT pixel for which ISOCAM yields $A_V = 43$ mag (at the ISOPHOT resolution), $I_{200\ \mu\text{m}} = 45$ MJy/sr and $I_{100\ \mu\text{m}} = 5$ MJy/sr. We have found that all the 100 μm emission comes from a thin outer layer ($A_V = 0\text{--}4$ mag) (using the standard *diffuse* dust emissivity, $\tau_{200\ \mu\text{m}} = 1.3 \times 10^{-25} \times N(\text{H})$, Draine & Lee 1984) while only 70% of the 200 μm emission comes from the same layer. The temperature of this layer drops from 16.5 to 10.4 K going inwards. Towards the core, there remains then 39 mag of cold dust to emit 30% of the 200 μm emission. Its average temperature is $\langle T_{\text{dust}} \rangle = 7.6 \pm 0.5$ K (taking into account a flat-field uncertainty of 8 MJy/sr and $\kappa_{200\ \mu\text{m}} = 0.18\text{--}0.34$ cm² g⁻¹ which applies for dense clouds, Ossenkopf & Henning 1994). Since it is an average, this is still an upper limit to the actual inner core temperature.

Because the core and the ridge are completely thick to UV–NIR emission, the thin and warm outer layer temperature depends merely on the radiation field coming from outside the cloud and not through it. Thus the outer layer properties should remain identical in front of the core and in front of the ridge. In the northern part of the ridge we measure $A_V = 30$ mag for a 49 MJy/sr flux at 200 μm . As for the core, subtracting the warm layer contribution, we find $\langle T_{\text{dust}} \rangle = 8.0 \pm 0.5$ K for the cold dust. The difference in temperature between the core and the ridge can be explained by the fact that the core is somewhat denser than the ridge. Indeed, Zucconi et al. (2001) show that the core temperature drops by 1 K for each tenfold density increase.

These results are compatible with the ISOCAM / MAMBO comparison. The ISOCAM data reach a peak extinction of $A_V \approx 125$ mag in an 11'' Gaussian beam towards the core (or 1.25×10^{23} cm⁻² using the standard conversion formula $N(\text{H}_2) \approx 10^{21} \times A_V$ cm⁻², Bohlin et al. 1978) and we measure a MAMBO flux of 23.3 MJy/sr (in the unsmoothed map). Dust temperatures in the range $T_{\text{dust}} = 7.0\text{--}9.0$ K can be derived from Eq. (1) of Motte et al. (1998) with a dust opacity in the

range $\kappa_{1200\ \mu\text{m}} = 0.006\text{--}0.01$ cm² g⁻¹. A detailed study of the dust will be presented in a future paper.

Acknowledgements. J. R. Pardo acknowledges support for his work from Spanish MCyT grant AYA 2000-1784, ESP 2002-01627, AYA 2002-10113-E. We thank A. Abergel and S. Cabrit for fruitful discussions and help. We thank J. Kirk, & D. Ward-Thompson for communicating their SCUBA data prior to publication. We thank both referees (D. Galli and D. Lemke) for fruitful discussions which helped to improve this Letter.

References

- Bacmann, A., André, P., Puget, J.-L., et al. 2000, A&A, 361, 555
 Bohlin, R. C., Savage, B. D., & Drake, J. F. 1978, ApJ, 224, 132
 Broguière, D., Neri, R., & Sievers, A. 1995, NIC Bolometer Users Guide (IRAM Int. Rep.)
 Cambrésy, L., Beichman, C. A., Jarrett, T. H., & Cutri, R. M. 2002, AJ, 123, 2559
 Draine, B. T., & Lee, H. M. 1984, ApJ, 285, 89
 Evans, N. J. II, Rawlings, J. M. C., Shirley, Y. L., & Mundy, L. G. 2001, ApJ, 557, 193
 Franco, G. 1989, A&A, 223, 313
 Gabriel, C., Acosta-Pulido, J., Heinrichsen, et al. 1997, in Proc. of the ADASS VI Conf., ed. G. Hunt, & H. E. Payne, ASP Conf. Ser., 125, 108
 Juvela, M., Mattila, K., Lehtinen, K., et al. 2002, A&A, 382, 583
 Lada, C. J., Lada, E. A., Clemens, D. P., & Bally, J. 1994, ApJ, 429, 694
 Laureijs, R. J., Clark, S. O., & Prusti, T. 1991, ApJ, 371, 602
 Laureijs, R. J., Fukui, Y., Helou, G., et al. 1995, ApJS, 101, 87
 Lehtinen, K., Mattila, K., Lemke, D., et al. 2003, A&A, 398, 571
 Miville-Deschênes, M.-A., Boulanger, F., Abergel, A., & Bernard, J.-P. 2000, A&AS, 146, 519
 Motte, F., André, P., & Neri, R. 1998, A&A, 336, 150
 Motte, F., Bontemps, S., et al., in prep.
 Ossenkopf, V., & Henning, T. 1994, A&A, 291, 943
 Pagani, L., Pardo, J.-R., Fich, M., Motte, F., & Stepnik, B. 2002, in Infrared and Submillimeter Space Astronomy, EAS Series, vol. 4, ed. M. Giard, et al. (Les Ulis: EDP Sciences), 145
 Pagani, L., Pardo, J.-R., Cambrésy, L., et al. 2003a, in Chemistry as a Diagnostic of Star Formation, ed. C. L. Curry, & M. Fich, in press
 Pagani, L., Pardo, J.-R., Motte, F., et al. 2003b, A&A, in prep.
 Teyssier, D., & Sievers, A. 1999, A Fast-Mapping Method for Bolometer Array Observations at the IRAM-30 m Telescope, IRAM technical note
 Ward-Thompson, D., Scott, P. F., Hills, R. E., & André, P. 1994, MNRAS, 268, 276 (WT94)
 Ward-Thompson, D., Kirk, J. M., Crutcher, R. M., et al. 2000, ApJ, 537, L135
 Ward-Thompson, D., André, P., & Kirk, J. M. 2002, MNRAS, 329, 257
 Zucconi, A., Walmsley, C. M., & Galli, D. 2001, A&A, 376, 650